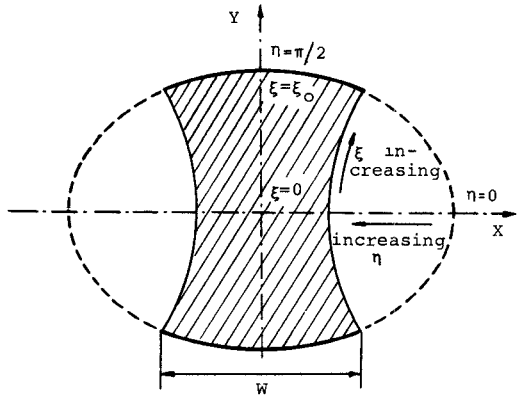

Fig. 2. Elliptic coordinate system and reflector guide as a cut section of closed elliptic waveguide.

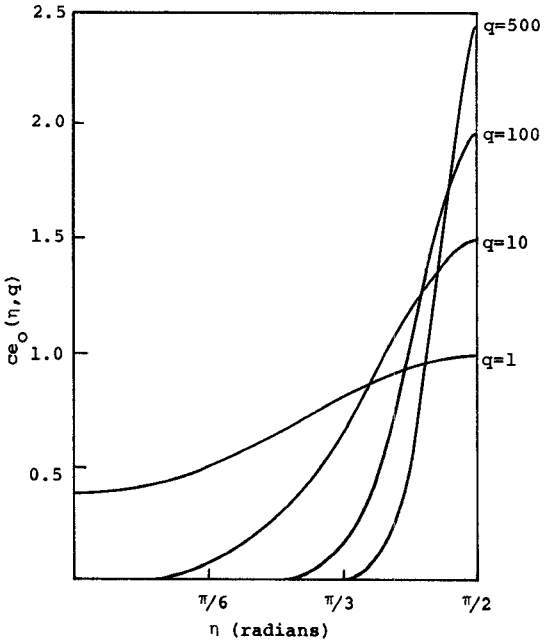

Fig. 3. Mathieu function $ce_0(\eta, q)$ versus angular coordinate η for various values of q (field distribution in X direction).

become concentrated in the region close to the Y axis ($\eta = \pi/2$) in the waveguide (Fig. 2). The degree of concentration increases with increasing value of q and, correspondingly, the magnitude of the electromagnetic field decreases rapidly with increasing distance from the Y axis. Hence, for large values of q, portions of the conducting wall of the elliptic waveguide can be removed in the regions where the field magnitude is negligible. This is indicated in Fig. 2 by the dashed parts of the elliptic boundary. What then remains is an open waveguide of width W with a cross section similar to that shown in Fig. 1 being turned around 90°. The field distribution in elliptic waveguides thus can be well used for the description of the fields in open waveguides for large values of q encountered for oversized dimensions of the distance D between the two cylindrical reflectors ($D \gg \lambda$). This requirement is always satisfied in practical open reflector-type waveguides.

COMPARISON OF THE RESULTS WITH THOSE OBTAINED BY OTHER APPROACHES

It was shown by Morse and Feshback [10] that for large values of the parameter q (large number of periods of the standing waves between the reflectors) the Mathieu functions ce_m and se_m can be approximated by series of Gaussian–Hermite functions as

$$ce_m(q,\eta) = A_m \sum_{\nu=-\infty}^{\infty} [\exp(-z_1^2/2)H_m(z_1) + \exp(-z_2^2/2)H_m(z_2)],$$

$$se_m(q,\eta) = B_m \sum_{\nu=-\infty}^{\infty} [\exp(-z_1^2/2)H_{m-1}(z_1) - \exp(-z_2^2/2)H_{m-1}(z_2)].$$

In these equations, we have

$$z_1 = (4q)^{1/4}(\eta - \pi/2 + 2\nu\pi)$$

$$z_2 = (4q)^{1/4}(\eta + \pi/2 + 2\nu\pi).$$

We observe that these functions for $m = 0$ are similar to those shown in Fig. 3. The series of Gaussian–Hermite functions, representing as an approximation the Mathieu functions, are identical to the functions found by considering wave propagation in the reflector guide based on the transverse wave-beam approach according to Schwering [1] and Nakahara [2].

REFERENCES

[1] F. Schwering, "Reiterative wave beams of rectangular symmetry," *Arch. Elek. Übertragung*, vol. 15, pp. 555–564, Dec. 1961.
[2] T. Nakahara and N. Kurauchi, "Guided beam waves between parallel concave reflectors," *IEEE Trans. Microwave Theory Tech.*, vol. MTT-15, pp. 66–71, Feb. 1967.
[3] J. E. Degenford, M. D. Sirkis, and W. Steier, "The reflecting beam waveguide," *IEEE Trans. Microwave Theory Tech.*, vol. MTT-12, pp. 445–453, July 1964.
[4] G. D. Boyd and J. P. Gordon, "Confocal multimode resonator for millimeter through optical wavelength masers," *Bell Syst. Tech. J.*, vol. 40, pp. 489–508, Mar. 1961.
[5] A. G. Fox and T. Li, "Resonant modes in a maser interferometer," *Bell Syst. Tech. J.*, vol. 40, pp. 453–488, Mar. 1961.
[6] L. A. Vainshtein, "Open resonators with spherical mirrors," *Sov. Phys.—JETP*, vol. 18, pp. 471–479, Feb. 1964.
[7] ——, *Open Resonators and Open Waveguides*. Boulder, Colo.: The Golem Press, 1969.
[8] L. J. Chu, "Electromagnetic waves in elliptic hollow pipes of metal," *J. Appl. Phys.*, vol. 9, pp. 583–591, Sept. 1938.
[9] J. G. Kretzschmar, "Wave propagation in hollow conducting elliptical waveguides," *IEEE Trans. Microwave Theory Tech.*, vol. MTT-18, pp. 547–554, Sept. 1970.
[10] P. M. Morse and H. Feshbach, *Methods of Theoretical Physics*, vol. II. New York: McGraw-Hill, 1953.
[11] G. Toraldo di Francia, "Flat-roof resonators," *Appl. Opt.*, vol. 4, pp. 1267–1270, Oct. 1965.

Surface Wave on a Ferrite Magnetized Perpendicular to the Interface

DALE F. VASLOW

***Abstract*—A semi-infinite ferrite magnetized perpendicular to the interface is found to support a nonmagnetostatic surface wave. The wave exists within a finite wavelength band and a finite frequency band. Since the wavelength is typically of the order of 1 cm, large samples of polycrystalline ferrite material may be used for the experiments.**

The propagation of magnetostatic surface waves on a ferrite slab magnetized in the plane of the slab and transversely to the direction of propagation has been studied theoretically [1] as well as experimentally [2], [3]. The effects on the magnetostatic surface wave produced by adding a conductive plate or a dielectric layer backed by a conductor to one side of the ferrite slab have also been investigated [4]–[6]. Morgenthaler [7] and Jao [8] have studied the propagation of magnetostatic surface waves on a ferrite slab magnetized transversely to the direction of propagation, but at an arbitrary angle θ to the ferrite slab surface. They found that for θ in the range $\theta_c < \theta < \pi - \theta_c$, where θ_c ($\theta_c < \pi/2$) is the critical angle, no magnetostatic surface wave exists. Nonmagnetostatic surface waves termed "dynamic mode" or "dielectrically induced" surface waves have been studied theoretically for a semi-infinite ferrite magnetized parallel to the interface and transversely to the direction of propaga-

Manuscript received July 26, 1973; revised January 28, 1974. This work was supported in part by the National Science Foundation under Grant GK-16203.
The author was with the Department of Electrical and Computer Engineering, University of Wisconsin, Madison, Wis. 53706. He is now with General Atomic Company, San Diego, Calif. 92138.

tion [9] and both theoretically and experimentally for an axially magnetized ferrite rod [10].

In this short paper, it is shown theoretically that a surface wave exists on a semi-infinite ferrite for $\theta = \pi/2$ (magnetostatic field perpendicular to the interface). Since the wavelength of this surface wave is of the order of the electromagnetic wavelength in the medium, the magnetostatic condition [11] is not satisfied, and electromagnetic induction cannot be ignored. This surface wave is a slow wave that exists over a finite wavelength band and a finite frequency band. The frequency band lies within the range of frequencies for which the main diagonal component μ_1 of the ferrite permeability tensor is negative. Since the wavelength is long (typically of the order of 1 cm), experiments will require large ferrite samples, much larger than have been used in magnetostatic surface-wave experiments. For such long wavelengths, however, the quality of the ferrite surface should be relatively less important, thus suggesting the use of polycrystalline ferrite material.

A plane interface $x = 0$ separates a vacuum (μ_0,ϵ_0) half-space $(x < 0)$ from a half-space $(x > 0)$ of ferrite $(\mu_0\boldsymbol{\mu}_r,\epsilon_0\epsilon_r)$ magnetized in the x direction. The relative permeability $\boldsymbol{\mu}_r$ of the ferrite is

$$\boldsymbol{\mu}_r = \hat{x}\hat{x} + \mu_1(\hat{y}\hat{y} + \hat{z}\hat{z}) + i\mu_2(\hat{y}\hat{z} - \hat{z}\hat{y}),$$

$$\mu_1 = [\Omega^2 - \Omega_H(\Omega_H + 1)]/(\Omega^2 - \Omega_H^2),$$

$$\mu_2 = \Omega/(\Omega^2 - \Omega_H^2),$$

$$\Omega = \omega/\omega_M,$$

and

$$\Omega_H = \omega_c/\omega_M,$$

where ω is the wave frequency, ω_c the gyromagnetic frequency, and ω_M the saturation magnetization frequency. Traveling waves in the y direction having the dependence of $f(x)\exp[i(k_M\eta y - \omega t)]$ are considered where η is the normalized wavenumber and $k_M = \omega_M/c = \omega_M(\mu_0\epsilon_0)^{1/2}$.

The application of Maxwell's equations to the fields in the ferrite region having the dependence $f(x) = \exp(ik_M\zeta x)$ results in the dispersion relation

$$A\zeta^4 + B\zeta^2 + C = 0 \tag{1}$$

where A, B, and C are defined in a previous communication [12]. In (1), ζ^2 has two solutions, ζ_1^2 and ζ_2^2. The two unique solutions $\zeta = \zeta_a$ and $\zeta = \zeta_b$, which satisfy the physical requirement of causality, are chosen from the four solutions $\pm\zeta_1$ and $\pm\zeta_2$ [12]. For the purposes of this short paper, as will be shown later, the correct choices for ζ_a and ζ_b are those that have positive imaginary parts. For this choice, the ferrite field amplitudes decay exponentially as $x \to \infty$. In the vacuum region, $f(x) = \exp(-ik_M\zeta_c x)$, where $\zeta_c = (\Omega^2 - \eta^2)^{1/2}$ for $\Omega > \eta$ and $\zeta_c = i(\eta^2 - \Omega^2)^{1/2}$ for $\eta > \Omega$. Note that ζ_c is chosen to have a positive imaginary part so that the vacuum field amplitudes decay as $x \to -\infty$.

The application of the boundary conditions that the tangential electric and magnetic fields be continuous across the vacuum–ferrite interface yields the following dispersion relation:

$$T_1 + T_2 + T_3 = 0 \tag{2}$$

$$T_1 = -\zeta_c(\zeta_a + \zeta_b)[\zeta_a\zeta_b - \epsilon_r(\eta^2 - \eta_2^2)] \tag{3a}$$

$$T_2 = (1 + \epsilon_r)\zeta_a\zeta_b(\eta^2 - \eta_7^2) \tag{3b}$$

$$T_3 = -(1 + \epsilon_r)(\eta^2 - \eta_2^2)(\eta^2 - \eta_6^2)(\Omega^2 - \Omega_5^2)/(\Omega^2 - \Omega_H^2) \tag{3c}$$

where

$$\eta_6^2 = [2\epsilon_r\Omega^2/(1 + \epsilon_r)](\Omega^2 - \Omega_2^2)/(\Omega^2 - \Omega_5^2)$$

$$\eta_7^2 = 2\epsilon_r\Omega^2/(1 + \epsilon_r)$$

$$\Omega_5 = (\Omega_H[\Omega_H + \epsilon_r/(1 + \epsilon_r)])^{1/2}$$

and

$$\eta_2 = \Omega(\epsilon_r)^{1/2}.$$

We shall denote by SW the regions of the Ω–η space where ζ_c is imaginary, and ζ_a and ζ_b are both imaginary or complex such that $\zeta_a = -\zeta_b^*$. Real solutions for the surface wavenumber η can be shown to arise from (2) only in the regions SW.

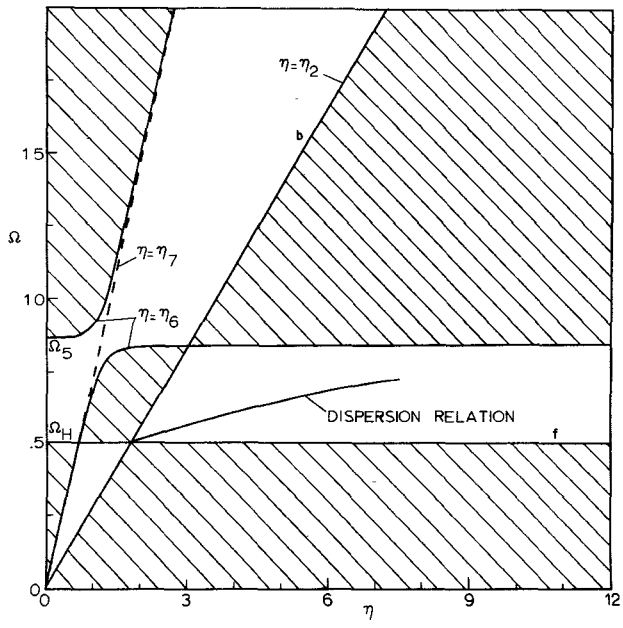

Fig. 1. Brillouin diagram of the surface wave for $\Omega_H = 0.5$ and $\epsilon_r = 13$. T_3 is negative in the shaded region.

The Brillouin diagram (Ω versus η space) in [12, fig. 1] shows the nature of ζ_a and ζ_b. Within the dotted area, bounded by curves d and e, ζ_a and ζ_b are complex and $\zeta_a = -\zeta_b^*$. In the areas shaded by horizontal (vertical) lines, $\zeta_a(\zeta_b)$ is real. The regions with no shading with dots and horizontal (vertical) lines correspond to ζ_a (ζ_b) being imaginary. The nature of ζ_c can also be represented on the Brillouin diagram by drawing a single straight line defined by $\eta = \Omega$. This line lies to the left of curve b. To the left of the line $\eta = \Omega$, ζ_c is positive real and to the right ζ_c is positive imaginary.

The regions of the Ω–η space where surface-wave solutions, that is, real solutions of (2) for η, can exist can be narrowed down further. In the regions SW, $\eta > \eta_2 > \eta_7$, which implies that T_1 and T_2 are negative. Consequently, the surface-wave dispersion relation (2) can have a solution only if T_3 is positive. In Fig. 1, the regions of the Ω–η space where T_3 is negative are shown by shaded lines. Clearly, no surface waves exist in these regions. Thus surface-wave solutions are possible only in those portions of the regions SW where T_3 is positive. Numerical search for the location of the wavenumber of the surface wave was restricted to these parts of the regions SW.

The dispersion relation for $\Omega_H = 0.5$ and $\epsilon_r = 13$ was obtained numerically and is shown as a line segment in Fig. 1. On the Brillouin diagram the dispersion relation begins at the intersection of $\eta = \eta_2$ and $\Omega = \Omega_H$ (curves b and f) and terminates on $\eta = \eta_3$ (curve a) [12]. For $\omega_M/2\pi = 5$ GHz, it is seen that the wavelength range is from 0.82 to 3.3 cm and the frequency range is from 2.5 to 3.64 GHz. The group delay time per unit length T_d is of the order of 1 ns/cm. T_d increases as the frequency increases for a fixed magnetic field strength but decreases as the magnetic field strength increases for a fixed frequency.

In conclusion, it has been shown theoretically that a surface wave exists on a semi-infinite ferrite magnetized perpendicular to the interface when the effect of electromagnetic induction is not neglected, as it is in the magnetostatic approximation. This surface wave is a slow wave that exists over a finite frequency band and a finite wavelength band. The frequency band lies within the range $\omega_c/2\pi < f < [\omega_c(\omega_c + \omega_M)]^{1/2}/2\pi$, where $\mu_1 < 0$. The wavelength is typically of the order of 1 cm, while a typical value for the group delay time per unit length is 1 ns/cm.

ACKNOWLEDGMENT

The author wishes to thank Prof. S. R. Seshadri for his assistance in the preparation of the manuscript.

REFERENCES

[1] R. W. Damon and J. R. Eshbach, "Magnetostatic modes of a ferromagnet slab," *J. Phys. Chem. Solids*, vol. 19, pp. 308–320, 1961.
[2] L. K. Brundle and N. J. Freedman, "Magnetostatic surface wave on a YIG slab," *Electron. Lett.*, vol. 4, pp. 132–134, 1968.

[3] J. D. Adam, "Delay of magnetostatic surface waves in YIG," *Electron. Lett.*, vol. 6, pp. 718–720, 1970.
[4] S. R. Seshadri, "Surface magnetostatic modes of a ferrite slab," *Proc. IEEE* (Lett.), vol. 58, pp. 506–507, Mar. 1970.
[5] W. L. Bongianni, "Magnetostatic propagation in a dielectric layered structure," *J. Appl. Phys.*, vol. 43, pp. 2541–2548, 1972.
[6] D. F. Vaslow, "Group delay time for the surface wave on a YIG film backed by a grounded dielectric slab," *Proc. IEEE* (Lett.), vol. 61, pp. 142–143, Jan. 1973.
[7] F. R. Morgenthaler, "A nonreciprocal magnetostatic surface wave independently controllable propagation and delay constants," *J. Appl. Phys.*, vol. 41, pp. 1014–1015, 1970.
[8] J. K. Jao, "Propagation of magnetostatic surface spin waves in YIG slabs," M.S. thesis, Mass. Inst. Technol., Cambridge, May 1971.
[9] J. P. Parekh and S. R. Ponamgi, "Dielectrically induced surface wave on a YIG substrate," *J. Appl. Phys.*, vol. 44, pp. 1384–1385, 1973.
[10] T. F. Tao, J. W. Tully, and F. W. Schott, "Dynamic mode surface waves on magnetized YIG and ferrite rods," *Appl. Phys. Lett.*, vol. 14, pp. 106–108, 1969.
[11] L. R. Walker, "Magnetostatic modes in ferromagnetic resonance," *Phys. Rev.*, vol. 105, p. 390, 1957.
[12] D. F. Vaslow and S. R. Seshadri, "Application of Brillouin diagram for a magnetized ferrite," *IEEE Trans. Antennas Propagat.* (Commun.), vol. AP-21, pp. 251–252, Mar. 1973.

RF Burnout of *Ku*-Band Mixer Diodes

GEORGE E. MORRIS, MEMBER, IEEE, AND GEORGE A. HALL

***Abstract*—This short paper describes the experiments conducted to determine the burnout capability of various types of *Ku*-band mixer diodes when subjected to narrow RF spikes. This condition results frequently in pulsed microwave systems where the receiver is not adequately protected or where the system's limiting devices degrade or fail.**

The maintenance problems resulting from mixer failures are severe and may become more so with increased usage of Schottky barrier diodes.

INTRODUCTION

Included in this study are four types of diodes all mounted in 1N78 type coaxial packages. These include 1N78C point contact, gold–germanium (AuGe)–gallium arsenide (GaAs) Schottky barrier,[1] palladium (Pd)–GaAs Schottky barrier,[1] and titanium–molybdenum–gold (Ti–Mo–Au)–silicon (Si) Schottky barrier. The criterion for failure was taken as a 1-dB increase in the 30-MHz IF noise figure. Failure at the 1-dB point was not considered valid unless there also occurred a corresponding decrease in diode crystal current. It was found that once the crystal current of a particular test diode decreased in an amount greater than 25 percent of the initial value that the diode could not recover but continued to degrade with increased incident power.

The diodes used for this study had noise figures in the following range. (Ti–Mo–Au)–Si Schottky barrier: 7.5–8.0 dB; (AuGe)–GaAs Schottky barrier: 6.5–7.0 dB; Pd–GaAs: 6.5–7.0 dB; and 1N78C's: 7.5–9.5 dB.

EXPERIMENTAL

To simulate near system environment, a pulse from an Army *Ku*-band PPS-5 radar operating at 16.2 GHz was transmitted through a gas transmit–receive (TR) tube without keep-alive. The radar pulse was about 1.2 kW in amplitude and 0.25 μs wide with a repetition rate of 4000 pulses/s. The resultant spike from the TR was approximately 1.5-ns duration and 30-W peak amplitude.

The maximum spike amplitude was determined by observing the deflection of a sampling oscilloscope through a calibrated attenuator and comparing this with the vertical deflections from known power sources. This scope calibration technique was accomplished with the aid of a variable precision attenuator, a temperature compensated thermistor, and a power bridge [1]. The experimental setup is shown in Fig. 1.

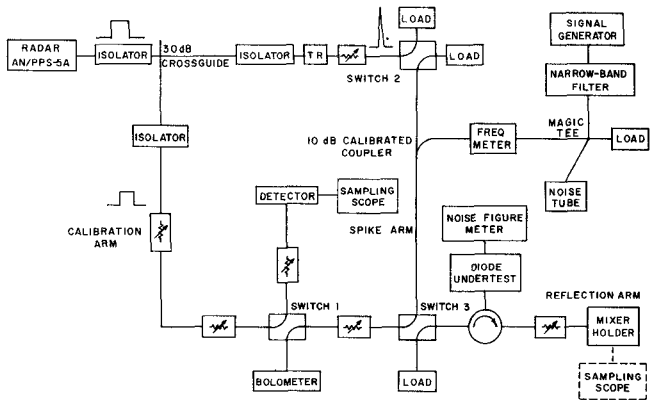

Fig. 1. Diagram of RF burnout test system.

Fig. 1 shows an 0.25-μs pulse emitted from the PPS-5 radar fed into a 30-dB cross-guide coupler. A small amount of this power is coupled into the calibration arm and is routed into the sampling scope by switch 1. The main portion of the 0.25-μs pulse hits the TR tube which emits leakage in the form of a narrow spike. This spike can either be dumped into a load by switch 2 or guided into the spike arm. Switch 3 allows the spike to enter into the calibration arm for determination of peak amplitude or into the arm containing the diode under test. The 10-dB coupler located in the spike arm allows power from the signal generator (LO source) and noise tube to be incident on the diode at the same time as the spike. The calibrated attenuator following the TR tube was used to adjust the incident spike levels for each test.

A complete burnout test for each diode consisted of the following. During this test, the diodes were mounted in a single ended (MA) model 595C Holder, and before each run, calibration of TR leakage was made. The incident power was adjusted to a low level (10–20 mW) and switched into the test diode. The peak reflected power, the noise figure, and the crystal current were monitored during the test period of 1 min (approximately 240 000 spikes). After this time period, the power was directed into a load by switch 2, and the diode's crystal current and noise figure were recorded. This procedure was repeated using the same diode with incremental increases in incident peak power until the diode failed.

Because the same diode was used for each power level test, the possibility of cumulative effects causing premature burnout was of concern to us. To check this possibility, a set of 1N78C point contact diodes were selected and divided into two groups. Diodes in group 1 were burned out using the procedure previously described. Once the typical burnout level was established, the second group was subjected to a one shot burnout test at this level. It was found that the diodes in group 2 had approximately the same number of failures as those diodes in group 1. It therefore seemed logical to assume that any cumulative effects resulting from narrow pulse energies were minor.

The spike amplitude emitted from a gas TR is not constant with time, and as a result, every transmitted pulse will not reach the maximum level [2]. For this reason, extreme care was taken during calibration to ensure that no spike exceeded a chosen deflection level with a constant attenuation setting. This was done by using the manual scan option on the sampling scope and photographing the spike for 2–3 min through an open shutter. The peak power data presented in Figs. 2 and 3 are the maximum amplitude spike referenced to the calibration amplitude observed before and after each diode run.

RESULTS

The burnout characteristics of the four types of diodes are presented in Figs. 2 and 3. Here, lots of 20 1N78C point contact and 24 (Ti–Mo–Au)–Si Schottky barrier diodes (Fig. 2) and 7 (Au–Ge)–GaAs Schottky barrier and 6 Pd–GaAs Schottky barrier diodes

Manuscript received August 17, 1973; revised January 17, 1974.
The authors are with the Semiconductor Devices and Integrated Electronics Technical Area, U. S. Army Electronics Technology and Devices Laboratory (ECOM), Fort Monmouth, N. J. 07703.
[1] Microwave Associates (MA) nomenclature designation MA 40538 (AuGe)–GaAs and MA 40539 Pd–GaAs diodes were received under Production Engineering Measure, U. S. Army Electronics Command, Fort Monmouth, N. J., under Contract DAAB05-69-C-0019, "Schottky-Barrier Gallium Arsenide Diodes," with MA.